Decay and dephasing of image-state electrons induced by Cs adsorbates on Cu(100) at intermediate coverage

A. K. Kazansky,[1,2,3] V. M. Silkin,[4] E. V. Chulkov,[4,5] A. G. Borisov,[2,3] and J.-P. Gauyacq[2,3]
[1]*Fock Institute of Physics, State University of Sankt Petersburg, Sankt Petersburg 198504, Russia*
[2]*CNRS, Laboratoire des Collisions Atomiques et Moléculaires, UMR 8625, Bâtiment 351, 91405 Orsay Cedex, France*
[3]*Université Paris-Sud, Laboratoire des Collisions Atomiques et Moléculaires, UMR 8625, Bâtiment 351, 91405 Orsay Cedex, France*
[4]*Donostia International Physics Center (DIPC), Paseo de Manuel Lardizabal, 4, 20018 San Sebastián/Donostia, Basque Country, Spain*
[5]*Departamento de Física de Materiales and Centro Mixto CSIC-UPV/EHU, Facultad de Ciencias Químicas, UPV/EHU, Apartado 1072, 20080 San Sebastián/Donostia, Basque Country, Spain*
(Received 8 January 2007; revised manuscript received 27 March 2007; published 7 June 2007)

A theoretical study of the influence of Cs adsorbates on the dynamics of Cu(100) image states is reported. It is applied to the coverage range where the Cs adsorbates are randomly adsorbed on the surface. In contrast to an earlier study based on a single adsorbate scattering approach and thus limited to the very low adsorbate coverages, the present work considers the image-state electron scattered by a given adsorbate in the presence of all the others. This allows the treatment of the intermediate coverage range. The core of the present approach consists of defining a coverage dependent potential representing the average interaction between the electron and the adsorbate layer together with a local perturbing potential centered on each adsorbate. A time-dependent study of electron scattering associated to a many-body treatment of inelastic interactions with bulk electrons yields the rates for population and coherence decay of the image-state electron. This leads to a discussion of the coverage dependence of the decay and dephasing rates, which exhibit a complex variation due to the simultaneous interactions of the image-state electron with many adsorbates on the surface.

DOI: 10.1103/PhysRevB.75.235412 PACS number(s): 73.20.−r, 73.50.Bk, 73.43.Cd, 79.60.−i

I. INTRODUCTION

Excited electronic states on surfaces are a subject of thorough theoretical and experimental research due to their fundamental and practical importance.[1–4] Among different excited states, the image potential states have received a lot of interest and form an appealing model system for studying the dynamics of electronic excitation at surfaces. Image potential states (ISs) appear on various surfaces as a consequence of the attraction between an electron located in vacuum and its image charge in the solid. Whenever electron penetration into the bulk is forbidden by the surface projected band gap, the image states form a Rydberg series converging to the vacuum level.[5–8] The electron motion in an image state is bound in the direction perpendicular to the surface and it is quasifree in the direction parallel to the surface. Thus the image states form two-dimensional continua and their energy is given by

$$E_n = -\frac{1}{32(n+a)^2} + \frac{k_\parallel^2}{2m^*},$$

where a is a quantum defect of the IS series, $k_\parallel$ is the electron momentum parallel to the surface, and m^* is an effective mass for the electron motion in the IS [unless stated otherwise, atomic units (a.u.) are used, i.e., $e^2=\hbar=m_e=1$]. Because of the weak coupling of the IS with the bulk, the effective mass for these states is very close to the free-electron mass.[9–12] Within the one-electron approximation the image states are stationary, i.e., they exhibit an infinitely long lifetime. However, in real materials the IS lifetime is finite due to inelastic interactions of the IS electron with the electrons in the solid. Since the wave functions of the ISs are mainly localized outside of the solid, the decay of an IS via electron-electron (e-e) interaction is rather slow.[13,14]

Due to their localization outside the solid surface, the ISs are substantially influenced by the quality of the surface. They are very sensitive to the presence of various surface defects. In particular, adsorbates, adatoms, vacancies, or steps can very efficiently scatter electrons in the image states. Along with intrinsic surface states, ISs can then be considered as useful tools to test the quality of a surface. The first observations of the influence of the presence of adsorbates on the characteristics of the surface localized states were reported by Kevan,[15] who used photoemission to study the occupied surface state on Cu(111) perturbed by potassium adsorbates. The broadening of the surface-state line in the emitted electron energy spectrum was found to vary linearly with the K adsorbate at low coverage. This was interpreted as the proof of the surface-state electron being scattered by adsorbates randomly distributed on the surface and an estimate of the scattering cross section by a single potassium adsorbate could be deduced. Effect of the adsorbates on the image states has been studied with two-photon photoemission spectroscopy. As a rule, ISs are empty at equilibrium. The first photon excites a metal electron into an IS and the second photon ejects the electron from this state into vacuum where both its energy and emission angle can be measured. Linear broadening of the IS spectral linewidth with increasing adsorbate coverage has been reported for several systems.[16–19]

The development of the femtosecond lasers created a broad research field with two-photon pump-and-probe experiments, in particular, for excited electronic states at surfaces such as ISs.[2,9,20–23] In these time-resolved two-photon

photoemission (TR-2PPE) studies, the first (pump) laser pulse excites an electron into an IS, and the second (probe) pulse ejects it into the continuum with a variable time delay. The spectra of ejected electrons are measured for various time delays. Thus the characteristics of the electron dynamics in the IS can be studied directly in the time domain. A number of pump-probe experiments of this type have been reported for ISs on adsorbate coated surfaces, where the change of the IS decay and dephasing times has been studied as a function of the adsorbate coverage. Particularly detailed studies are available for Cu/Cu(100) and CO/Cu(100) systems.[9,22,24–26] This makes important and timely the development of a deep theoretical understanding of how various properties of a surface can influence the IS characteristics.

Recently a theoretical treatment of the IS electron scattering by a set of adsorbates randomly distributed on the surface has been developed. It considers that the IS electron is scattered independently and incoherently by the various adsorbates. It thus describes the IS dynamics via the scattering properties of a single adsorbate on the surface. It has been applied to a few different adsorbates: alkalis, Ar, and Cu.[27–31] Two different scattering processes of the IS electron have been identified: interband and intraband scattering. If the recoil of the adsorbate is neglected, both scattering processes are energy conserving. In an interband scattering process, the IS electron is scattered into a band of electronic states different from the initial one (another IS, bulk band, or surface state if available); this corresponds to a population decay of the image state. Intraband scattering corresponds to the scattering of the image-state electron inside an IS continuum, i.e., to a mere change of direction of $k_{\parallel}$. It leads to the pure dephasing process. These two processes can be linked to the parameters T_1, T_2, and T_2^* entering optical Bloch equations[32] commonly used to analyze TR-2PPE experimental data.[2] The population decay process involving interband scattering determines the T_1 decay time. The coherence decay process involving intraband scattering determines the pure dephasing time T_2^*. Both processes contribute to the total line broadening given by $1/T_2$. In the limit of low adsorbate coverage of the surface, one can assume that the IS electron is scattered independently and incoherently by each adsorbate; this leads to population and coherence decay rates of the IS that vary linearly with the adsorbate coverage (see the discussion in Ref. 28). In this case, the scattering potential is the one induced by a single adsorbate. This approach, which leads to the linear variation of dephasing and broadening rates as functions of the coverage, is termed the "single adsorbate approach" below. One can stress that such a scattering approach relies on a random distribution of adsorbates on the surface. The situation would be quite different in the case of adsorbate clustering into islands. Then, scattering of the IS electrons by the adsorbate clusters and/or the island edges has to be considered.

The practical implementation of the single adsorbate approach, relying upon the independent scattering of an IS electron by a single adsorbate, is limited to the low coverage cases. For higher coverages this simple theory has to be revised. Let us consider the case of alkali adsorbates studied below.

Electron transfer from a single alkali adsorbate to the metal substrate together with the screening of the resulting charge results in a strong dipole field outside the surface. This field can influence ISs over a large region of space surrounding the adsorbate. When the coverage is not so small, the fields from different adsorbates overlap and one cannot consider that the IS electron is scattered independently by each adsorbate and collective effects appear. The dipole fields of all the adsorbates influence collectively the IS electron, though each adsorbate still acts as a scattering center. It is the aim of the present work to develop a theoretical approach of the IS dynamics that can be applied to the intermediate adsorbate coverage range. This approach takes into account (i) the collective effect of the long-range dipolar fields of all the adsorbates above the surface, and (ii) electron scattering by the short-range part of the potential around individual adsorbates.

The paper is organized as follows. In Sec. II we detail our theoretical approach. Results of the calculations for the IS decay and dephasing rates are presented in Sec. III. Finally, Sec. IV is devoted to summary and conclusions.

II. METHOD

An approach suitable for intermediate coverages has to consider the effects from all the adsorbates collectively. A first step in this direction has been performed in Ref. 33. An effective potential $V_{eff}(z)$ has been defined, which represents the mean interaction between an electron and all the alkali adsorbates. Computed from the dipoles located on each adsorbate, $V_{eff}(z)$ is a function of only z, the distance along the surface normal. It is independent of $\vec{\rho}$, the position vector parallel to the surface. In the limit of very large z, this effective potential is equal to $\Delta\Phi$, the change of the surface work function induced by the alkali adsorbates. Including the averaged effective potential $V_{eff}(z)$ in the Schrödinger equation describing the IS, one redefines "dressed" image states on the averaged adsorbate-modified surface. The average potential changes the IS energies adjusting them automatically to the work function of the adsorbate-modified surface. This approach was found[33] to account very well for the energy of the IS in the Na/Cu(111) system as a function of the adsorbate coverage measured by Fischer *et al.*[34] The maxima of the dressed IS wave functions were found to shift away from the surface as the alkali coverage is increased.[33] Together with the change of the energy of the ISs that places them deeper into the projected band gap of Cu(111), the shift of the maxima of the IS wave functions leads to a decrease of the IS penetration inside the bulk. Consequently, this should lead to a decrease of the IS decay rate due to inelastic interactions with the Fermi sea of bulk electrons.

The dressed image states are defined through the $V_{eff}(z)$ potential. However, the complete potential corresponding to the electron interaction with all the adsorbates on the surface can still lead to scattering of the IS electrons, induced by the difference between the complete potential and the average $V_{eff}(z)$ potential. Since the long-range dipolar part of the electron-adsorbate interaction is taken care of by $V_{eff}(z)$, the effective scattering potential becomes a sum of very weakly overlapping short-range potentials V_{Sc} localized around each adsorbate. This is quite different from the interaction with a

single adsorbate, where the scattering potential presents a long-range dipolar part. Together with a noticeable shift of the maximum of the IS electron wave function into the vacuum side,[33] this makes the reduced interaction between the IS electron and adsorbed atom much weaker. The above redefinition of the scattering potential for the dressed image states opens the way to the treatment of the dynamics of ISs at intermediate coverage on the base of single-scattering theory developed earlier for very low adsorbate coverage. Indeed, the single-scattering approach relies on the independent scattering from individual adsorbates so that the scattering cross section cannot exceed the mean distance between adsorbates. Note, however, that the present approach is computationally very demanding. For each adsorbate coverage one has to (i) obtain $V_{eff}(z)$, and a scattering potential V_{Sc}; (ii) obtain the dressed states as the unperturbed scattering states defined by the $V_{eff}(z)$ potential; (iii) finally, calculate the scattering of the dressed image-state electron by V_{Sc}. The results of the present approach should smoothly join the earlier single adsorbate scattering results as the coverage decreases. At the same time, one expects that this treatment will reveal a new behavior of the IS decay and dephasing processes as functions of adsorbate coverage, different from the linear behavior found at very low coverage.

In the following, we consider the case of the IS on a Cu(100) surface perturbed by Cs adsorbates. The reason for choosing this system is twofold: (i) Cs adsorbates are very efficient scatterers and thus collective effects should appear easily; (ii) there is a complete Rydberg series of the ISs on Cu(100) and their dynamics is not affected by the proximity of the upper projected band-gap edge. At the $\bar{\Gamma}$ point, the projected band gap of Cu(100) (X gap) extends from −3.11 to +2.98 eV (all the energies are given with respect to the vacuum level). Therefore a complete Rydberg series of ISs converging to the vacuum level exists with the energies $E_1=-0.573$ eV, $E_2=-0.177$ eV, $E_3=-0.084$ eV, etc. There is no surface state on the (100) surface of Cu at the $\bar{\Gamma}$ point, but there is a surface resonance at approximately −3.5 eV. The above energies are obtained with the model potential[35] used in the present study and are very close to the experimental data for the clean Cu(100) surface.

A. Definition of the potentials

When a single alkali atom is adsorbed on a metal, its valence electron is transferred into the substrate. The resulting charge is screened by the metal leading to the formation of a dipolar field around the adsorbate. The presence of the screening charge makes it difficult to define the charge state of an adsorbate, the total system being neutral (see a discussion in Scheffler *et al.*[36]). However, both two-photon-photoemission experiments and theoretical studies on alkali adsorbates reveal an unoccupied adsorbate-induced resonance with an energy well above the Fermi level.[37] This resonance has been shown to originate from the valence orbital of the alkali atom. One can thus consider a single alkali atom to be ionized on a metal surface and to be accompanied by its screening charge. When coverage is increased, depolarization of the adsorbates sets in, reducing the dipole localized on each adsorbate. The equilibrium adsorption height of Cs/Cu(100) is $Z_{Ads}=3.0$ a.u. measured from the image reference plane as can be deduced from low-energy electron-diffraction (LEED) experiments[38] or extracted from the coverage dependence of the surface work function.[39] In our study limited to the coverage range where the work function varies linearly with coverage, we assumed the adsorbate charge and adsorption distance to be constant. The work-function shift induced by the adsorbate layer is $\Delta\Phi=-4\pi\eta q Z_{Ads}$, where q is the charge of the adsorbate ($q=+1$. in the present study). The surface density of adsorbates, η, can be related to the coverage $\theta=\eta/\eta_0$, where η_0 is the surface density of Cu atoms [$\eta_0=0.043$ a.u.$^{-2}$ for Cu(100)].

We use cylindrical coordinates with the z axis perpendicular to the surface and going through the center of a given adsorbate. Positive values of z correspond to the electron being in vacuum. The potential describing the electron interaction with a single adsorbate is defined as

$$U_{Ads}(\rho,z) = U_0(\rho,z-Z_{Ads}) - \frac{1}{\sqrt{\rho^2+(z-Z_{Ads})^2}} + \frac{1}{\sqrt{\rho^2+(z+Z_{Ads})^2}},$$

$$U_{Ads}(\rho,z) = 0, \quad z \leqslant 0, \tag{1}$$

where the electron radius vector is $\vec{r}=(\vec{\rho},z)$, and Z_{Ads} is the distance between the adsorbate and the image plane located at $z=0$. The adsorbate potential is assumed to be completely screened inside the metal. The pseudopotential $U_0(\rho,z)$ has been obtained from the l-dependent potential introduced by Bardsley[40] to describe alkali atoms. It contains local and nonlocal terms in the Kleinman-Bylander form[41] (see Ref. 27 for an explicit definition). The Coulomb contribution from the positive core is absent from $U_0(\rho,z)$ and represented by a separate term (second term in the equation). Therefore $U_0(\rho,z)$ is a short-range potential. The third term stands for the interaction of the electron with the electrostatic image of the adsorbate core. The sum of the second and third terms results in the long-range dipolar potential induced by the alkali adsorbate.

The total potential induced by the adsorbate layer is obtained as the sum of the electron interactions with individual adsorbates:

$$U_T(\vec{\rho},z) = \sum_j U_{Ads}(|\vec{\rho}-\vec{\rho}_j|,z), \tag{2}$$

where $\vec{\rho}_j$ give the positions of randomly distributed adsorbates. $U_T(\vec{\rho},z)$ depends on the distribution of the adsorbates over the surface, but $U_T(\vec{\rho},z=\infty)$ is equal to the change of the surface work function $\Delta\Phi$. At low and moderate coverage (below about two-thirds of the saturation coverage), there is no long-range order in the Cs adsorbates, both at low and at room temperature, and the Cs adatoms are distributed as an isotropic fluid with short-range order.[42]

It is very difficult to take into account the stochastic distribution of the adsorbates in a real situation and we resorted to a model approach. The model is defined both by the sys-

tem considered and by the averaging procedure used to generate the effective potential below. The best model of the adsorbate distribution over the surface should be chosen through minimizing the square of the fluctuations of some physical quantities averaged over an ensemble of stochastically sampled adsorbates. However, this formidable task is much beyond the scope of the present paper. In the present work, we use a potential $V_{Av}(\rho,z)$ resulting from an average of the total potential created by the dipoles associated with alkali adsorbates at the surface. Inside the Wigner-Seitz cell surrounding an adsorbate, we performed averages over circles of radius ρ centered at the adsorbate [the radius ρ is then smaller than the Wigner-Seitz radius $\rho_{WS}=(\pi\eta)^{-1/2}$]:

$$V_{Av}(\rho,z) = U_0(\rho,z-Z_{Ads}) + V_{Dip}(\rho,z), \tag{3}$$

where

$$V_{Dip}(\rho,z) = \left\langle \sum_j \left(-\frac{1}{\sqrt{(\vec{\rho}-\vec{\rho}_j)^2+(z-Z_{Ads})^2}} + \frac{1}{\sqrt{(\vec{\rho}-\vec{\rho}_j)+(z+Z_{Ads})^2}} \right) \right\rangle_{|\vec{\rho}|=\rho}. \tag{4}$$

Thus the averaging in Eq. (3) is performed using only the dipolar part of the electron interaction potential with a single adsorbate. Considering that the $U_0(\rho,z-Z_{Ads})$ contributions from different adsorbates are short ranged and that the dipolar part is long range, one can conclude that the potential $V_{Av}(\rho,z)$ is close to what one would expect from the average of the total potential $U_T(\vec{\rho},z)$ inside the Wigner-Seitz cell. In our computations, we assumed that the adsorbates are sampled on a hexagonal lattice, and the averaging procedure corresponds to averaging over all the configurations obtained by rotation around the z axis which passes through the selected adsorbate.

The next step is to define the effective potential $V_{eff}(z)$. Following earlier work,[33] we define it as the one-dimensional potential $V_{eff}(z)=V_{Dip}(\rho_{WS},z)$. It represents the average action of the adsorbate layer and, at infinity, it joins the correct asymptote of the total adsorbate-layer induced potential $V_{eff}(\infty)=\Delta\Phi$ and $V_{eff}(z\leqslant 0)=0$. Note that a few possible ways of constructing $V_{eff}(z)$ have been considered in earlier work.[33] In particular, we compared the energies and wave functions of the ISs obtained with different effective potentials: (i) the total potential averaged over the Wigner-Seitz circle in a hexagonal lattice, (ii) the potential above the central hollow position in a hexagonal lattice, and (iii) the potential above the central hollow point in a square lattice. These various definitions of the average potential appeared to lead to extremely similar results and this gives confidence in the present procedure using an average over a hexagonal lattice. One can stress that the effective potential only relies on the dipoles associated with the adsorbates. It obviously depends on the specific adsorbate considered via the value of the equilibrium adsorption height Z_{Ads}.

We can then rewrite the average potential given in Eq. (3) to explicitly include the effective potential:

$$V_{Av}(\rho,z) = U_0(\rho,z-Z_{Ads}) + \underbrace{[V_{Dip}(\rho,z)-V_{eff}(z)]}_{\Delta V(\rho,z)} + V_{eff}(z) \tag{5}$$

so that the average potential, $V_{Av}(\rho,z)$, appears as the effective potential plus a perturbation. The latter is located inside the Wigner-Seitz cell surrounding the adsorbate. Following its definition, the perturbing potential vanishes at the edge of the Wigner-Seitz cell. Taking this into account, we now define the model potential $V(\rho,z)=V_{Av}(\rho,z)+V_{Surf}(z)$ for the electron moving within the dressed image state as

$$\begin{aligned} V(\rho,z) &= U_0(\rho,z-Z_{Ads}) + \Delta V(\rho,z) + V_{eff}(z) + V_{Surf}(z), \\ &\rho \leqslant \rho_{WS}, \quad z>0, \\ V(\rho,z) &= U_0(\rho,z-Z_{Ads}) + V_{eff}(z) + V_{Surf}(z), \\ &\rho > \rho_{WS}, \quad z>0, \\ V(\rho,z) &= V_{Surf}(z), \quad z\leqslant 0, \end{aligned} \tag{6}$$

where $V_{Surf}(z)$ is the model potential describing the electron interaction with the clean Cu(100) surface. It has been introduced by Chulkov *et al.*[35] and adjusted to the experimental properties of the Cu(100) surface at the $\bar{\Gamma}$ point. This potential is only a function of the electron coordinate perpendicular to the surface thus a free-electron motion parallel to the surface is assumed. The present approach does not include the relaxation of the substrate induced by the alkali adsorption and its possible effect on a scattering of the IS electrons.

The model potential given by Eq. (6) describes the following scattering process. The dressed image state appears as an eigenstate of the Hamiltonian for electron motion perpendicular to the surface:

$$\mathcal{H}_\perp = -\frac{1}{2}\frac{d^2}{dz^2} + V_{Surf}(z) + V_{eff}(z). \tag{7}$$

The electron within the two-dimensional (2D) continuum of the dressed image state is moving parallel to the surface and is scattered by the short-range adsorbate-induced potential $V_{Sc}(\rho,z)=U_0(\rho,z-Z_{Ads})+\Delta V(\rho,z)$. This scattering process leads to the decay and dephasing of the dressed image state. Since the effective scattering potential is localized in both ρ and z directions, one can attempt to compute the broadening and decay of the new dressed image states within the one-center approximation.[27] Observe that, for each coverage, the asymptotic scattering channels given by ISs have to be redefined together with the adsorbate-induced scattering potential. In particular, the energy positions of the ISs become coverage dependent.

Figure 1 presents the results obtained for the energies of the first three ISs on Cu(100) as functions of Cs coverage on the surface. The general behavior of the eigenstates and eigenfunctions is described in Ref. 33. In particular, it was shown that, in the case of Na adsorbates on Cu(111), the present approach only using the effective potential $V_{eff}(z)$ accurately reproduces the experimental IS energies for work function decreases up to 0.7 eV. In the present study, we take the same limit for the work-function change (0.7 eV).

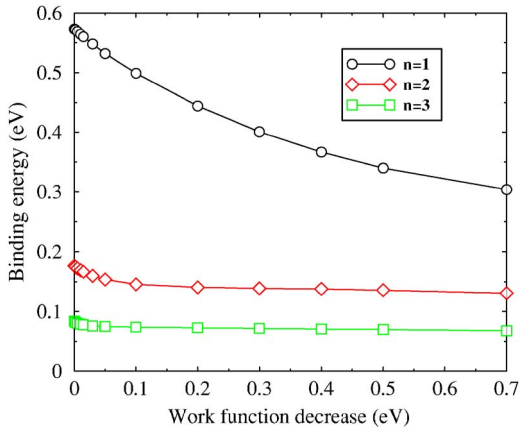

FIG. 1. (Color online) Binding energy of the first three image states on Cs/Cu(100). The energies of the levels are given in eV as functions of the work function decrease induced by the Cs adsorbates. Open circles: $n=1$; open diamonds: $n=2$; open squares: $n=3$. Lines are given as guides for the eye.

B. Multielectron interactions

The dressed states computed in the previous section vary with coverage. In particular, the maxima of the corresponding wave functions move toward vacuum as the adsorbate coverage is increased. The change of the wave functions of the ISs together with the change of their energy leads to the decrease of the IS penetration inside the bulk Cu.[33] One can then expect a decrease of the IS decay due to inelastic interactions with bulk electrons. This problem has been addressed within the framework of many-body theory. The essential details of this approach can be found in Refs. 3 and 14. Briefly, the damping rate due to inelastic scattering, Γ_n^{e-e}, of an electron characterized by energy $\varepsilon_n > E_F$ and wave function χ_n is obtained in the "on the energy-shell" approximation as the projection of the imaginary part of the nonlocal self-energy operator onto the electron state itself (see, for instance, Refs. 14 and 43)

$$\Gamma_n^{e-e} = -2\int d\mathbf{r}\int d\mathbf{r}'\,\chi_n^*(\mathbf{r})\,\mathrm{Im}\,\Sigma(\mathbf{r},\mathbf{r}';\varepsilon_n)\chi_n(\mathbf{r}'). \quad (8)$$

Here, the wave functions of the image states χ_n as well as the bulk wave functions $\phi_i(z)$ have been obtained as the eigenfunctions of the Hamiltonian given by Eq. (7), which incorporates the effective potential of the adsorbate layer. In the so-called GW approximation for the self-energy, the first term in the series expansion in terms of the screened Coulomb interaction $W(\mathbf{r},\mathbf{r}';\omega)$ is retained only. Then $\mathrm{Im}\,\Sigma$ is evaluated in terms of W and of the final states $\phi_f(\mathbf{r})$ allowed for the decay process:

$$\Sigma(\mathbf{r},\mathbf{r}';\varepsilon_n) = \sum_{E_F \le \varepsilon_f \le \varepsilon_n} \phi_f^*(\mathbf{r}')\,\mathrm{Im}\,W(\mathbf{r},\mathbf{r}';\varepsilon_n-\varepsilon_f)\phi_f(\mathbf{r}). \quad (9)$$

Here the summation is performed over the final-state energies which are between the initial state and the Fermi energy. The screened interaction W is given in linear-response theory by the equation (in short notation)

$$W = v + (v + K_{\mathrm{xc}})\chi v, \quad (10)$$

where v is the bare Coulomb potential and $\chi(\mathbf{r},\mathbf{r}';\omega)$ is the linear density response function for the interacting electron system. The latter is obtained from the following integral equation (in short notation):

$$\chi = \chi^o + \chi^o(v + K_{\mathrm{xc}})\chi. \quad (11)$$

The kernel K_{xc} entering Eqs. (10) and (11) accounts for the reduction of the electron-electron interaction due to exchange and correlation effects. Present calculations have been performed in the so-called random-phase approximation when K_{xc} is set equal to zero in both Eqs. (10) and (11). In Eq. (11) $\chi^o(\mathbf{r},\mathbf{r}';\omega)$ is the density response function of the noninteracting electron system:

$$\chi^o(\mathbf{r},\mathbf{r}';\omega) = 2\sum_{i,j}\frac{\theta(E_F-\varepsilon_{i\mathbf{q}_i})-\theta(E_F-\varepsilon_{j\mathbf{q}_j})}{\varepsilon_{i\mathbf{q}_i}-\varepsilon_{j\mathbf{q}_j}+(\omega+i\eta)} \times \phi_i(\mathbf{r})\phi_j^*(\mathbf{r})\phi_j(\mathbf{r}')\phi_i^*(\mathbf{r}'). \quad (12)$$

In this equation η is an infinitesimally small positive constant and in the present calculations has been put equal to 1 meV. The summation over i,j also includes image states. We assume that the one-electron energies $\varepsilon_{i\mathbf{q}_i}$ have the parabolic form

$$\varepsilon_{i\mathbf{q}_i} = \varepsilon_i + q_i^2/2m_i \quad (13)$$

with band index i dependent effective masses to reproduce bulk projected electronic structure of Cu(100) surface. The further calculation details can be found in Ref. 44.

C. Scattering by the adsorbates

The next step is to study the scattering of an electron initially in the asymptotic state associated with the n_0-th dressed image state by the axially symmetric potential $V_{Sc}(\rho,z)$. This problem is addressed using the scattering approach developed in Refs. 27–29, of which we only give a brief overview here. Scattering of the IS electron by an adsorbate can be described with the following stationary Schrödinger equation:

$$E\Psi(\vec{\rho},z;E) = \left(-\frac{1}{2}\Delta + V(\rho,z)\right)\Psi(\vec{\rho},z;E), \quad (14)$$

where $V(\rho,z)$ is given by Eq. (6). The asymptotic behavior of $\Psi(\vec{\rho},z;E)$ at $\rho\to\infty$ is given by

$$\Psi(\vec{\rho},z;E) \sim \exp(i\vec{k}_{n_0}\vec{\rho})\chi_{n_0}(z) + \sum_{n=1}\mathcal{A}_{n_0\to n}(k_{n_0},\varphi)\frac{\exp(ik_n\rho)}{\sqrt{\rho}}\chi_n(z) + \int d\varepsilon\,\mathcal{A}_{n_0\to\varepsilon}(k_{n_0},\varphi)\frac{\exp(ik_\varepsilon\rho)}{\sqrt{\rho}}\chi_\epsilon(z). \quad (15)$$

Here φ is the azimuthal angle ($\varphi=0$ is along the direction of the incident electron parallel to the surface); $\chi_n(z)$ is the eigenfunction of the nth dressed IS, i.e., the eigenfunction of

the Hamiltonian given by Eq. (7). The total energy E is the sum of the eigenenergy of the dressed IS, ε_n, and of the translational energy of the IS electron parallel to the surface, $k_n^2/2$. In the incident channel $E=\varepsilon_{n_0}+k_{n_0}^2/2$. In the asymptotic region, summation over n includes the open IS channels, i.e., such that $\varepsilon_n \leqslant E$. The integral term corresponds to the possible transitions into the bulk states. Obviously, the functions $\chi_\epsilon(z)$ in Eq. (15) obey outgoing (into the bulk) boundary conditions. Equations (14) and (15) are written under the implicit assumption that the adsorbate is immobile during the scattering process, i.e., adsorbate recoil is neglected. This is justified by the very large mass ratio between the adsorbate and the scattered electron, which makes the energy transfer very small. As a consequence, electron scattering by the adsorbate is always elastic (energy conserving).

Due to the axial symmetry of the problem, the component of the electron angular momentum normal to the surface m is a good quantum number and the wave function can be expanded as

$$\Psi(\vec{\rho},z;E)=\sum_{m=-\infty}^{\infty}\psi_m(\rho,z;E)e^{im\varphi}. \tag{16}$$

The problem (14) becomes then a set of independent 2D scattering problems for various values of m:

$$E\psi_m(\rho,z;E)=\underbrace{\left(-\frac{1}{2\rho}\frac{\partial}{\partial\rho}\rho\frac{\partial}{\partial\rho}+\frac{m^2}{2\rho^2}+V(\rho,z)\right)}_{\mathcal{H}_m}\psi_m(\rho,z;E); \tag{17}$$

with the asymptotic behavior at $\rho\to\infty$,

$$\psi_m(\rho,z;E)\sim\frac{1}{2}\left(H_m^{(2)}(k_{n_0}\rho)\chi_{n_0}(z)-\sum_n \mathcal{B}_{n_0\to n}^{(m)}(k_n)H_m^{(1)}(k_n\rho)\chi_n(z)\right), \tag{18}$$

where $H_m^{(1)}(x)$ $[H_m^{(2)}(x)]$ are the Hankel function of first (second) kind. The scattering amplitude $\mathcal{A}_{n_0\to n}(k,\varphi)$ is given by

$$\mathcal{A}_{n_0\to n}(k,\varphi)=\frac{1}{\sqrt{2\pi k_{n_0}}}\sum_{m=-\infty}^{\infty}(\mathcal{B}_{n_0\to n}^{(m)}(k_n)+\delta_{n,n_0})i^m e^{im\varphi}. \tag{19}$$

The 2D-scattering problem has been solved with a nonstationary method[27,45] where the time-dependent Schrödinger equation with Hamiltonian $\mathcal{H}_m$ is solved on a grid of points in cylindrical coordinates. The time evolution of a wave packet $\Psi_m(\rho,z;t)$ is thus obtained for an initial wave function given by the Gaussian wave packet:

$$\Psi_m(\rho,z;t=0)=e^{-ik_0\rho}e^{-[(\rho-\alpha)/\gamma]^2}\chi_{n_0}(z). \tag{20}$$

A single run allows us to extract the scattering properties within a given energy range. The latter is adjusted with parameters k_0, α, and γ. Provided the time-dependent solution $\Psi_m(\rho,z;t)$ is known, the quantities $\mathcal{B}_{n_0\to n}^{(m)}(k_n)$ are obtained in the asymptotic region of space. The virtual detector method is used.[27,28,46] For a fixed coverage, the nonstationary computations are to be run for each value of m and for all the ISs of interest.

From the calculated $\mathcal{B}_{n_0\to n}^{(m)}(k_n)$ we can now determine decay and dephasing rates. Inter-band transitions between ISs correspond to $n\neq n_0$. These transitions contribute to the decay of the n_0 IS. The corresponding rate constant $\gamma_{n_0\to n}$, the product of the scattering cross section by the initial velocity of the electron in the IS, is given by

$$\gamma_{n_0\to n}=\sum_{m=-\infty}^{\infty}|\mathcal{B}_{n_0\to n}^{(m)}(k_n)|^2,\quad n\neq n_0. \tag{21}$$

Partial rate constants corresponding to a given m value can also be defined by only retaining one term in the summation in Eq. (21). It is noteworthy that, when written in atomic units, this quantity corresponds to a scattering probability. The decay rate of the IS due to the $n_0\to n$ transition is given by

$$\Gamma_{n_0\to n}=\eta\gamma_{n_0\to n}+\Gamma_{n_0\to n}^{e-e},\quad n\neq n_0, \tag{22}$$

where η is the surface density of adsorbates. The first part is the adsorbate scattering contribution and the second one is the contribution of inelastic electron-electron interactions. Note that Eq. (22) links the two quantities, "rate constants" and "rates," which are discussed below.

The total decay rate of the IS should be computed by summing the interband transitions to all possible final states. Such a direct computation is difficult because of the transitions to the continuum of the bulk states. The unitarity relation provides a more convenient way for finding the total decay rate constant γ_{n_0} and the total decay rate $\Gamma_{n_0}^{(decay)}$:

$$\gamma_{n_0}=\sum_{m=-\infty}^{\infty}[1-|\mathcal{B}_{n_0\to n_0}^{(m)}(k_{n_0})|^2], \tag{23}$$

$$\Gamma_{n_0}^{(decay)}=\eta\sum_{m=-\infty}^{\infty}[1-|\mathcal{B}_{n_0\to n_0}^{(m)}(k_{n_0})|^2]+\Gamma_{n_0}^{e-e}. \tag{24}$$

Similarly we define the rate constant for intraband transitions, i.e., for elastic scattering of the electron inside the n_0-th image state continuum:

$$\gamma_{n_0\to n_0}=\sum_{m=-\infty}^{\infty}|1+\mathcal{B}_{n_0\to n_0}^{(m)}(k_{n_0})|^2. \tag{25}$$

In this process the electron is remaining in the same IS, but changes its direction of motion parallel to the surface. The population of the IS is not changed by such a transition, but the quantal state of the electron is changed within the same continuum (change of direction of $k_\parallel$). Alternatively, one can say that intraband scattering corresponds to the broadening of an initial plane wave into a distribution in momentum space. This intraband scattering process thus corresponds to a decay of the coherence of the IS, i.e., to the pure dephasing process. One can stress that in a quantum-mechanical framework, elastic scattering is associated with an additional phase (usually called the phase shift) to the quantal state, acquired

TABLE I. Contribution of inelastic electron-electron interactions to the decay rate $\Gamma_n^{e\text{-}e}$ of the $n=1$ and $n=2$ ISs. The calculations are performed at the $\bar{\Gamma}$ point for various values of the work function change $\Delta\Phi$ induced by the Cs adsorbates. P_n is the penetration probability of the nth IS inside bulk Cu. For $n=2$, $\Gamma_{2\to1}^{e\text{-}e}$ is the partial decay rate associated to the inter-IS band transitions (from $n=2$ to $n=1$).

$\Delta\Phi$, eV	P_1	$\Gamma_1^{e\text{-}e}$, meV	$\Gamma_1^{e\text{-}e}/P_1$, meV	P_2	$\Gamma_2^{e\text{-}e}$, meV	$\Gamma_{2\to1}^{e\text{-}e}$, meV	$\Gamma_2^{e\text{-}e}/P_2$, meV
0.0	0.052	16.11	310	0.0093	3.58	0.46	385
−0.05	0.051	15.82	310	0.0082	3.14	0.40	383
−0.1	0.050	15.30	306	0.0072	2.73	0.34	379
−0.2	0.046	13.93	303	0.0062	2.29	0.26	369
−0.3	0.041	12.43	303	0.0060	2.14	0.22	357
−0.4	0.036	10.84	301	0.0060	2.08	0.20	347
−0.5	0.032	9.29	290	0.0061	2.05	0.18	337
−1.0	0.015	3.95	263	0.0056	1.66	0.12	296

in the collision, that motivates the term of dephasing (see discussions in Refs. 28 and 47). The total broadening rate due to both decay and dephasing is then obtained as

$$\Gamma_{n_0}^{(broadening)} = \eta\gamma_{n_0\to n_0} + \Gamma_{n_0}^{(decay)}. \tag{26}$$

Within the single adsorbate approach, one makes the assumption that electron scattering by a given adsorbate is independent of scattering by all the others, so that the various rates are proportional to the adsorbate surface density. This approach is limited to the case when the scattering cross section is smaller than the distance between two adsorbates (see discussion in Refs. 27–29). In the present alkali adsorbate case, the scattering cross sections by a single adsorbate are quite large, restricting the validity domain of the single-scattering adsorbate approach to very small coverages. The present development remedies this difficulty by redefining both the IS and the scattering potential. The latter is confined inside the Wigner-Seitz cell surrounding a given adsorbate, so one can expect that, at least classically, the cross section is smaller than the average distance between adsorbates. In this framework, scattering by each adsorbate is localized and can be computed independently from the others. One thus obtains rates given by Eqs. (22), (24), and (26) that contain the adsorbate density as a factor. However, due to the coverage dependence of the scattering process, the dependence of the rates on the coverage is nontrivial.

One then expects the present "dressed IS" approach to remedy the problems of the "single adsorbate" approach, though retaining a scattering formalism. Two consistency checks are discussed below: (i) comparison of the scattering cross sections with their geometrical limit given by the average adsorbate-adsorbate distance; (ii) comparison of the present results with those of the single-scattering approach in the limit of very low coverage. The limitation of the present dressed IS approach comes from the definition of the $V_{eff}(z)$ and $V_{Sc}(\rho,z)$ potentials it relies upon. In the present work, they are derived from the pseudopotential of an individual unperturbed adsorbate, together with its screening charge. When the adsorbate coverage increases, adsorbates influence each other, leading, e.g., to the depolarization of the layer and to a decrease of the adsorbate dipole. In this case, our approach would have to be modified to accommodate this change of the electron interaction with individual adsorbate. In practice, this limits our approach to the coverage range where the adsorbate-induced work function change varies linearly with coverage.

III. RESULTS

Table I presents the results for the contribution of inelastic electron-electron interactions in the bulk to $\Gamma_n^{e\text{-}e}$, the decay rate of the $n=1$, and $n=2$ ISs. The calculations are performed at the $\bar{\Gamma}$ point, i.e., at the bottom of the IS continuum and for various values of the work function change $\Delta\Phi$ induced by the Cs adsorbates. The contribution of the inter-IS band transitions (from $n=2$ to $n=1$) is shown for the decay of the $n=2$ IS. As follows from the present results, the inter-IS transitions appear to contribute to around 10% to the decay of the $n=2$ IS. We took this study as an opportunity to further check the link between penetration and decay induced by inelastic interactions in the bulk. Within a simple model,[6] the inelastic decay rate of the ISs should be proportional to the probability to find the IS electron inside bulk Cu (penetration probability) given by $P_n=\int_{-\infty}^{0}\chi_n^2(z)dz$. As seen in Table I from the ratio $\Gamma_n^{e\text{-}e}/P_n$, the width $\Gamma_n^{e\text{-}e}$ is not exactly proportional to the penetration factor. Though the deviation remains rather limited (at most 17% for the $n=1$ IS), and the penetration approximation thus yields a reasonable estimate in this case.

As expected, with increasing Cs coverage, or, equivalently, with decreasing work function the penetration of the ISs inside bulk Cu drops. This results in a significant decrease of the $\Gamma_n^{e\text{-}e}$ decay rate. This is a direct consequence of the change of the IS binding energy induced by the Cs adsorbates: on the average, the IS electron is moving further away from the Cs/Cu(100) surface and thus interacts less efficiently with the bulk electrons. The sensitivity of the decay rates for the two $n=1$ and $n=2$ IS on Cs coverage is quite similar.

Figures 2 and 3 present some results of the scattering calculations and illustrate the change of the Cs scattering properties as a function of the surface coverage. The results

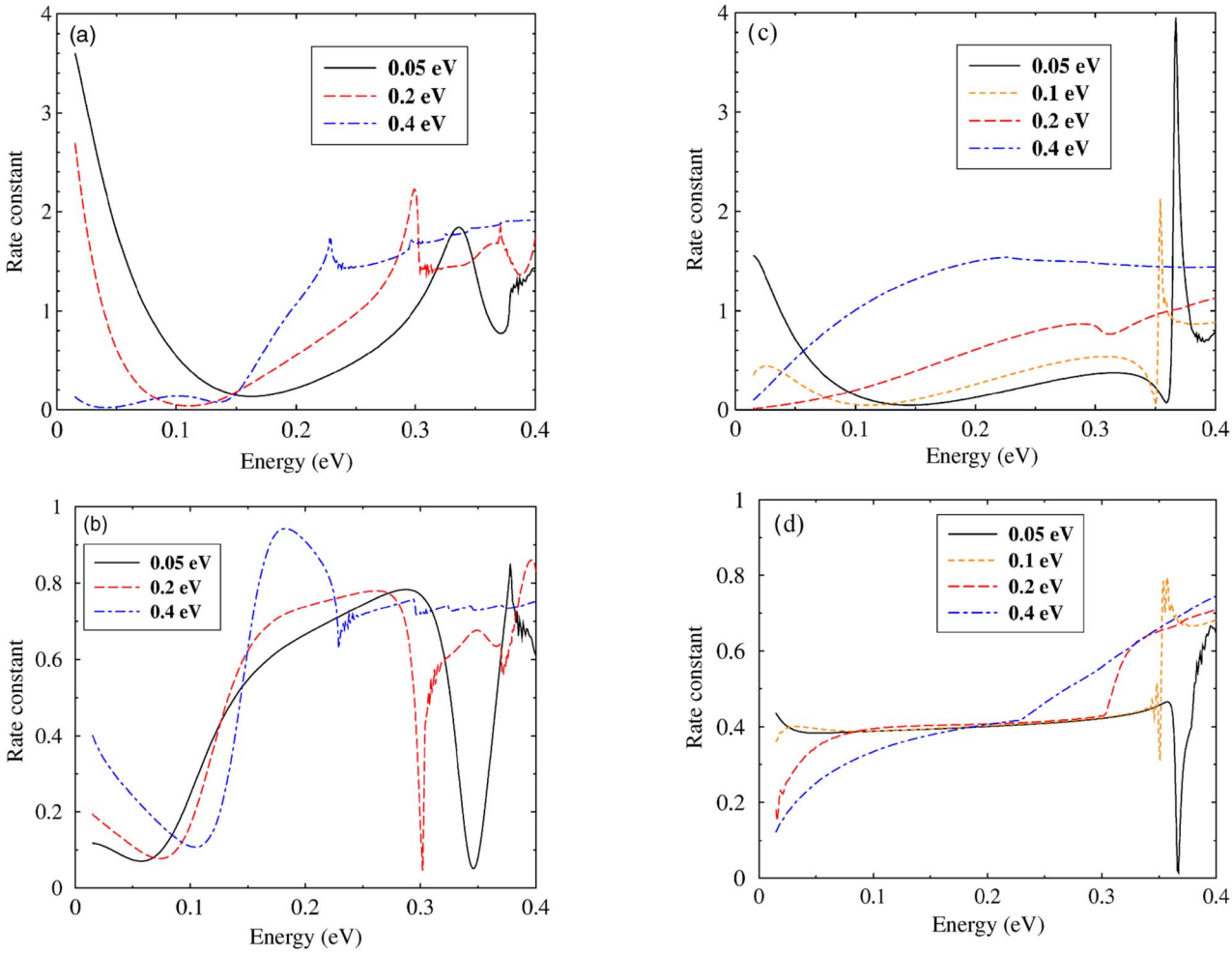

FIG. 2. (Color online) (a) Rate constant (in atomic units) for intraband scattering in the $m=0$ symmetry of the $n=1$ IS on a Cu(100) surface partly covered by Cs adsorbates. The rate constant is presented as a function of energy of the electron motion parallel to the surface, i.e., with respect to the bottom of the $n=1$ continuum. Three different coverages are shown that correspond to the work-function decrease equal to 0.05 eV (full black line), 0.2 eV (red dashed line), and 0.4 eV (blue dash-dotted line). (b) Same as (a), but for interband scattering of the $n=1$ IS in the $m=0$ symmetry. (c) Same as (a) for intraband scattering of the $n=1$ IS in the $m=1$ symmetry. Four different coverages are shown that correspond to the work-function decrease equal to 0.05 eV (full black line), 0.1 eV (orange dotted line), 0.2 eV (red dashed line), and 0.4 eV (blue dash-dotted line). (d) Same as (c), for interband scattering of the $n=1$ IS in the $m=1$ symmetry.

in Fig. 2 span a range of work-function change between 0.05 and 0.4 eV, corresponding to a Wigner-Seitz radius ρ_{WS} between 80.8 and $28.6a_0$. Figure 2 presents the partial rate constants for intraband and interband scattering for the $n=1$ IS in the $m=0$ and $m=1$ symmetry. The rate constants are shown as functions of the kinetic energy of the electron motion parallel to the surface, i.e., with respect to the bottom of the IS continuum. Because of prohibitively large computing time for studying very low-energy scattering within the nonstationary approach (see, e.g., Ref. 27), the present results are limited to the energies above 15 meV. Similarly, the high-frequency oscillations visible in partial rate constants close to the thresholds for the higher n IS are artifacts due to the finite wave-packet propagation time that introduces some inaccuracies in the treatment of the slow electron outgoing in the higher n IS channels.

As a first remark, the changes in the scattering properties when the coverage increases are significant, in particular for intraband scattering. The general idea is that the procedure described in Sec. II A results in a weakening of the scattering potential as the coverage increases. In addition, the range of action of the scattering potential, $V_{Sc}(\rho,z)=U_0(\rho,z-Z_{Ads})+\Delta V(\rho,z)$, is strongly limited to the Wigner-Seitz cell and as a consequence it decreases with increasing coverage. The main features of the rate constant as a function of the electron kinetic energy have been discussed in Ref. 27. The various structures are due to the opening or closing of the higher-lying IS channels and due to quasistationary states of the system. The latter are a consequence of the two-dimensional character of the IS continuum perturbed by an adsorbate-induced scattering potential. Indeed, in two dimensions, a potential that is attractive on the average is always able to carry a bound state in the $m=0$ symmetry.[48] Its binding energy is exponentially small, if the potential is weak. The present problem is not purely two dimensional, and therefore this mathematical statement is not rigorously valid here. However, loosely bound states associated with 2D localization around adsorbed species were found in various similar

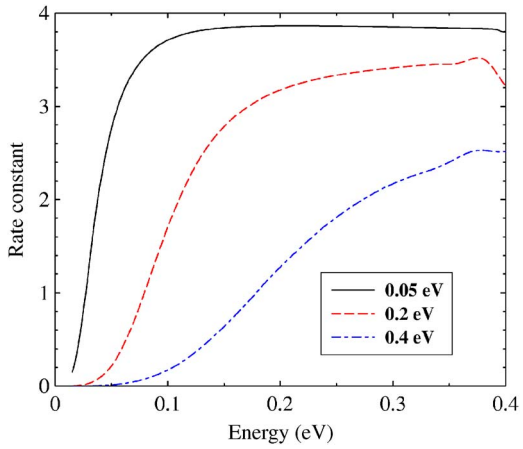

FIG. 3. (Color online) Rate constant (in atomic units) for intraband scattering in the $m=2$ symmetry of the $n=1$ image state on a Cu(100) surface partly covered by Cs adsorbates. The rate constant is presented as a function of the energy of the electron parallel to the surface, i.e., with respect to the bottom of the $n=1$ continuum. Three different coverages are shown corresponding to work-function decreases equal to 0.05 eV (full black line), 0.2 eV (red dashed line), and 0.4 eV (blue dashed-dotted line).

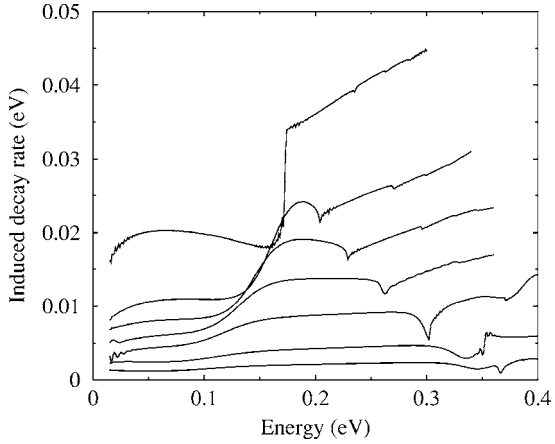

FIG. 4. Decay rate of the $n=1$ image state on Cu(100) induced by various amounts of Cs adsorbates on the surface. The decay rate (in eV) is presented as a function of the energy of the electron motion parallel to the surface, i.e., with respect to the bottom of the $n=1$ continuum. The different curves correspond to different Cs coverages of the surface, associated to work-function changes of 0.05, 0.1, 0.2, 0.3, 0.4, 0.5, and 0.7 eV. One can recognize the various curves in the figure by noticing that the decay rate is larger for larger work-function change.

systems both in theoretical approaches[49–53] and experimental scanning tunnel microscopy (STM) and photoemission studies.[53–56] Due to the actual 3D nature of the problem, these states arising from the localization of 2D continua appear as quasistationary states since they can decay into the 3D-bulk continuum. The localization effect turns out to be a common feature in the alkali-adsorbate–noble-metal systems. For example, in the intraband scattering in $m=0$ symmetry in Fig. 2, the peak around 0.33 eV for $\Delta\Phi=0.05$ eV is due to such a quasistationary state. It appears as a bound state for the $n=2$ IS continuum (it is located below the energy of $n=2$ IS at $\bar{\Gamma}$) and can decay into the $n=1$ IS continuum and into the bulk states, influencing scattering of $n=1$ IS electrons. As the Cs coverage increases, the corresponding peak in Fig. 2 decreases in intensity and shifts down in energy, while remaining below the $n=2$ threshold. This is not surprising, since when the coverage increases, the effective potential around an adsorbate weakens and the bound state becomes more weakly bound. The peak at zero energy in the intraband scattering in $m=0$ symmetry was also attributed[27] to such a quasistationary state hidden below the $n=1$ IS threshold. In that case, it arises from the $n=1$ IS localization. The importance of this state in the scattering process is also seen to weaken as the Cs coverage increases.

The strong and sharp structure in the intraband rate constant in the $m=1$ symmetry near the $n=2$ threshold deserves to be mentioned. In this case, a repulsive centrifugal potential $\frac{m^2}{2\rho^2}$ exists, but the attractiveness of the Cs adsorbate is strong enough for the localization of a bound state below the $n=2$ continuum. This quasistationary state disappears as the coverage increases, it transforms into a resonance in the $n=2$ continuum, which appears to be too broad to influence scattering.

In contrast to the intraband scattering induced by the long-range part of the scattering potential, the interband scattering is mainly due to the short-range part of the scattering potential (see discussion in Refs. 28 and 29). This appears very clearly in the single adsorbate case where the m convergence of interband transition probability is much faster than that of intraband scattering.[28,29] In the present study the range of the scattering potential is limited inside the Wigner-Seitz cell. The reduction of the range of the scattering potential with increasing coverage is well illustrated in Fig. 3 which shows the rate constant for intraband scattering of $n=1$ electrons in the $m=2$ symmetry. Note that in this case, due to the strong centrifugal potential, there is no quasistationary state. The rate constant at low energy quickly decreases as coverage increases. Scattering in a high m angular wave, such as $m=2$, is mainly sensitive to the long-range part of the potential resulting in this fast drop. This feature is not visible for the $m=0$ and $m=1$ waves, which are able to penetrate deeply into the potential and experience the effect of short-range forces (as, e.g., illustrated by the $n=2$ localization found in $m=1$ symmetry). The weaker sensitivity of the interband rate constant to the presence of Cs adsorbates has also to be linked to the weak dependence of the short-range part of the scattering potential on the Cs coverage in the present approach.

The total, i.e., summed over m, rate of the $n=1$ IS decay induced by scattering on Cs adsorbates is presented in Fig. 4 as a function of the electron energy with respect to the $n=1$ image-state band bottom. Results are shown for different values of the work-function change. One can see that globally the IS decay rate induced by scattering is increasing as the Cs coverage increases, though its evolution is complex: its increase is not homogeneous and depends on the electron kinetic energy. As the main visible feature, one can mention the structure below the $n=2$ threshold reflecting the localization of the $n=2$ continuum in the $m=0$ symmetry. For low coverage, the quasistationary state induces a broad dip in the

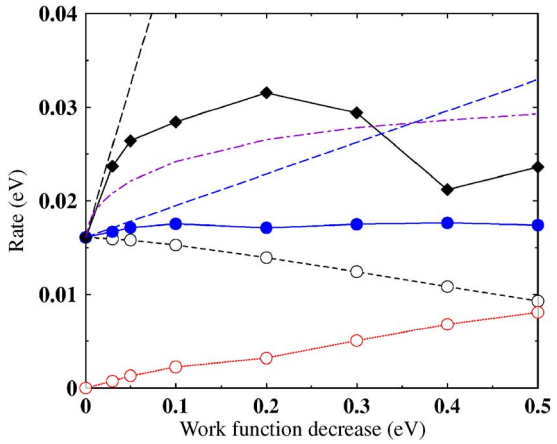

FIG. 5. (Color online) Rates for the evolution of the $n=1$ image state on Cu(100) in the presence of Cs adsorbates. The rates are presented as a function of the work-function decrease induced by the Cs adsorbates. The energy is 0.015 eV above the bottom of the $n=1$ continuum. Population decay rates: total decay rate (blue full line and full circles), contribution from electron-electron interactions (short-dashed black line and open circles), decay induced by scattering on the adsorbates (dotted red line and open circles). Total broadening rate: black full line with full diamonds. Geometric limit for the total broadening rate: dash-dotted line. The two long dashed lines present the linear behavior of the decay and broadening rates obtained in the single adsorbate scattering approximation.

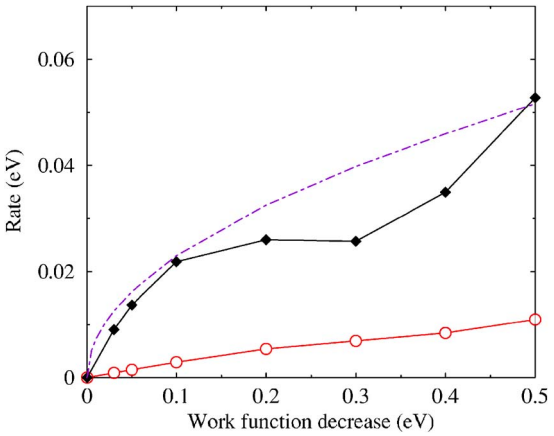

FIG. 6. (Color online) Rates for the evolution of the $n=1$ image state on Cu(100) induced by scattering on Cs adsorbates. The rates are presented as a function of the work-function decrease induced by the Cs adsorbates. The energy is 0.1 eV above the bottom of the $n=1$ continuum. Population decay induced by scattering: red full line and open circles. Broadening induced by scattering: black full line with full diamonds. Geometric limit for the total broadening rate: dashed-dotted line.

decay rate which moves down in energy while narrowing as the coverage is increased. Its effect disappears for a work-function change $\Delta\Phi=0.7$ eV where it is replaced by a sharp step in the decay rate located at the $n=2$ IS threshold.

Using the above results on inelastic electron-electron interactions and on Cs scattering, we can now derive the total rates for population decay, dephasing, and broadening of the ISs in the presence of Cs adsorbates. These rates are, e.g., the ones used in optical Bloch equation analysis of a time-resolved photoemission experiment. Besides their interest as the actual quantities governing the IS dynamics, the total rates also provide the basis for a consistency check of our treatment: comparison with the single adsorbate approach results and with the geometrical limit. In Fig. 5 results of the present calculations for the $n=1$ IS continuum are shown for the energies close to $\bar{\Gamma}$. (For computational reasons, the scattering terms have been actually evaluated at 15 meV above the continuum bottom.) Let us first consider the population decay rate (circles): the scattering contribution (red dotted-line with open circles) is seen to increase with the Cs coverage whereas the inelastic electron-electron interaction contribution (black dashed line with open circles) is decreasing. As a result, the population decay rate of the $n=1$ IS (blue full line with full circles) appears to be roughly constant with coverage. Figure 5 also shows the estimate obtained in the single adsorbate approach; the corresponding straight line (blue dashed line) agrees with the present finite coverage results only at very small coverages. In this case, the upper limit of validity of the single adsorbate approach can be estimated to be in the range of 10^{-3} monolayers (MLs), corresponding to a work-function change of $\Delta\Phi\approx-0.04$ eV. The full black line with diamonds corresponds to the total broadening rate obtained in this study for the $n=1$ IS. Similarly to the decay rate, the present result for broadening is much smaller than what would be predicted by an extrapolation of the single adsorbate results. The validity of the single adsorbate approach is again seen to be restricted to the 10^{-3}-ML range. However, if one only considers the scattering contribution, it appears that the effect of the redefinition of the scattering potential for the dressed ISs is stronger on the broadening rate than on the decay rate. This confirms once more that the present redefinition of the scattering potential as a function of Cs coverage is mainly influencing the long-range part of the potential and thus the dephasing of the ISs rather than the decay of their population.

Figure 5 presents another consistency check of the present approach. A scattering description of the effect of adsorbates on the IS is only valid as long as the scattering cross section is smaller than the distance between two adsorbates. The geometrical limit for the broadening rate is then obtained as

$$\Gamma_{limit}^{(broadening)} = k_{\parallel}\sqrt{\eta} + \Gamma_n^{e-e}. \tag{27}$$

This geometrical limit (dashed-dotted line in Fig. 5) is seen to be of the order of magnitude of the calculated broadening rate. This confirms *a posteriori* the consistency of our approach. In the present case, broadening rates above the geometrical limit can be attributed to quantal effects: a quantal scattering cross section can be larger than the geometrical size of the scattering potential. It follows from the geometrical limit, that, in the present system, the $n=1$ total broadening rate at the bottom of the continuum cannot increase much compared to its value on the clean surface. This is exactly the result found in the present scattering approach.

Figure 6 presents a further illustration of the effect of the geometrical limit. It shows the rates of the adsorbate-induced decay and broadening of the $n=1$ IS for 100-meV kinetic energy of the IS electron motion parallel to the surface (the

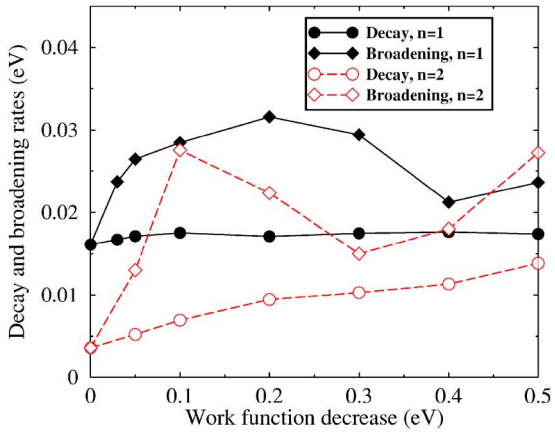

FIG. 7. (Color online) Rates for the evolution of the $n=1$ and $n=2$ image states on Cu(100) in the presence of Cs adsorbates. The rates are presented as a function of the work-function decrease induced by the Cs adsorbates. The energy is 0.015 eV above the bottom of the $n=1$ continuum. Circles: decay rate; diamonds: broadening rates. Full line and full black symbols: $n=1$ state. Dashed line and open red symbols: $n=2$.

contribution from inelastic electron-electron interactions is not included). The decay rate induced by scattering increases almost linearly with coverage, again due to the weak dependence of the short-range forces on coverage. As for the broadening rate, the results of the scattering calculations are very close to the geometrical limit. However, in this case, the geometrical limit allows a significant increase of the broadening rate with coverage.

Figure 7 presents a comparison for the population decay and broadening rates for the $n=1$ and $n=2$ ISs at the bottom of the corresponding IS continua. Results are shown as a function of the work-function change induced by Cs adsorbates. The rates for the $n=2$ IS appear to be much more sensitive to Cs coverage than the ones for the $n=1$ IS. In particular, the decay rate exhibits an almost linear dependence on the adsorbate coverage. This is very close to the behavior predicted in the single adsorbate approximation (not shown here) for $|\Delta\Phi|$ smaller than 0.2 eV. The difference between the coverage dependence of $n=1$ and $n=2$ decay rates is mainly due to the $\Gamma_n^{e\text{-}e}$ contribution: it is weaker for $n=2$ and its variation cannot balance that of the scattering contribution. Similarly, the broadening rate for $n=2$ is increasing by around a factor 7 in the studied work-function range, i.e., a significant increase compared to the weak increase for the $n=1$ IS. One can stress that the geometrical limit is the same for all the different ISs and, the decay and broadening rates for $n=2$ are smaller than those for $n=1$ on a clean surface, but they both reach the same magnitude for $\Delta\Phi=-0.5$ eV.

To our knowledge, no experimental results are available for the IS in the Cs/Cu(100) system. However, another alkali-metal–noble-metal system, Na/Cu(111) has been studied by 2PPE.[19,34] The coverage dependence of the IS energy computed in the present approach nicely accounts for the detailed measurements of Fischer *et al.*[34] (see in Ref. 33). No time-dependent measurements were performed and only linewidths have been reported. Fischer *et al.*[34] reported an IS linewidth roughly constant with coverage and a factor 2 larger than that on the clean surface. In contrast, Wang *et al.*[19] reported a linewidth quickly increasing with coverage, the IS disappearing above 0.012 ML. Though a detailed comparison is impossible, we can notice that the linear behavior observed for $n=1$ in the present results at low coverage ($|\Delta\Phi|<0.05$ eV) is of the order of 9 eV/ML, i.e., of the same order of magnitude as the linewidth variation reported by Ref. 19, 12 eV/ML for Na/Cu(111) at $\bar{\Gamma}$. The results obtained for Na/Cu(111) in the single adsorbate scattering approach are slightly smaller of the order of 4–5 eV/MLs.[28] In addition, one can also stress that the Cs/Cu(100) and Na/Cu(111) systems might lead to different behaviors: Na adsorbates are less efficient scatterers than Cs and the position of the upper edge of the Cu projected band gap inside the IS spectrum on (111) surfaces influences their variation.

At this point, we can go back to the various approximations involved in the present study. First, the dressed image states are obtained from the effective average potential, $V_{eff}(z)$. The derivation of the latter makes use of a hexagonal adsorbate ordering on the surface, which is not expected to be always the case. However, detailed tests have shown that different assumptions for the alkali lattice lead to very similar $V_{eff}(z)$ potentials and to very similar IS energies,[33] giving confidence in the present approach. Second and more importantly, the inhomogeneities in the distribution of adsorbates on the surface can lead to an inhomogeneous broadening of the ISs because of mesoscopic fluctuations in their energy positions. This can be also expected to lead to other scattering processes, the IS being scattered by a more or less local inhomogeneity of $V_{eff}(z)$. These inhomogeneities can appear both in the distribution of adsorbates on the surface and in the distribution of adsorbate heights. Short-range inhomogeneities can be expected to contribute to dephasing more effectively than the decay of the IS. Indeed, decay occurs by short-range scattering on an individual adsorbate and it is thus independent of the global phase of the wave function accumulated on a large piece of the surface. It could, however, depend on the adsorption height. On the contrary, dephasing can be enhanced by the stochastic phase accumulation in collisions with a number of adsorbate atoms. To our knowledge, the contribution of these inhomogeneities to the IS dynamics has not been addressed in the literature.

IV. CONCLUDING SUMMARY

We have reported a theoretical study of the dynamics of the image potential states on the adsorbate coated metal surface. The rates of the adsorbate-induced decay and dephasing of the ISs were calculated for variable Cs coverage on the Cu(100) surface. While earlier treatments were based on a single adsorbate scattering approach[27] and thus limited to the very low adsorbate coverage range, the present approach enables us to address the case of intermediate coverages. It takes into account the effect of all the other adsorbates on the scattering properties of a given adsorbate. The basic idea of our method is to define an average smooth potential resulting from the action of all the adsorbates and to study scattering

induced by the difference between the total potential and this smooth average potential. In a way, we define dressed IS taking into account the presence of an adsorbate layer and compute the scattering by an individual adsorbate. This has also the advantage of including the surface work-function change induced by the adsorbates. The method is applied to the case of Cu(100) surface coated with Cs adsorbates, the latter being very efficient scattering centers for the ISs.

The main results follow:

Similarly to the clean metal surface case, image states on a metal surface with adsorbates decay by inelastic many-body electron-electron interactions. However, an additional decay channel opens due to elastic interband scattering of the IS electron on the adsorbates. Intraband scattering on the adsorbates leads to the loss of the coherence of the ISs.

The penetration inside bulk Cu of the dressed image states decreases as the adsorbate coverage increases. This leads to a significant decrease of the many-body inelastic decay rate of the ISs.

The present scattering results are quite different from the ones obtained in the single adsorbate approach. This effect is particularly strong in the present system due to the scattering efficiency of Cs adsorbates. The variation of the decay and dephasing rates of the IS with the adsorbate coverage deviates very quickly from the linear behavior found in the single adsorbate approach (for the $n=1$ IS the deviation appears in the 10^{-3}-ML coverage range).

Decay and mainly dephasing rates induced by scattering on the adsorbates are found to be reduced by the introduction of dressed image states. The variation of the decay and dephasing rates with the adsorbate coverage is much slower than the linear behavior exhibited at very low coverage. Nevertheless, very quickly as the Cs coverage increases, the IS broadening is dominated by the scattering processes, contrary to the clean surface case where inelastic electron-electron interactions dominates.

In a scattering approach, the IS total scattering cross section has to be smaller than the average distance between adsorbates. This leads to a geometrical limit of the IS broadening induced by scattering on the adsorbates. The present results do fulfill this condition. Actually, for the $n=1$ IS, this severely limits the increase of the IS broadening with Cs coverage.

For a given adsorbate, one then expects decay and dephasing rates to vary linearly with coverage in the low coverage range; this linear variation saturates above a certain limit, when collective effects appear. The limit between the two regimes (single adsorbate and dressed IS scattering) depends on the scattering properties of the adsorbates. Weak scatterers like Cu adatoms on Cu(100) allow for a linear variation of the IS rates over a large coverage range,[9,22,25,26] which can be well described in the single adsorbate approach.[30,31] Similarly, CO adsorbates on Cu(100) also exhibit a linear variation of decay and dephasing rates over a significant coverage range; in this case, a saturation of the decay and dephasing rates as functions of coverage has been observed around 0.15 ML.[24] In contrast, efficient scatterers like Cs are associated to a low limit and theoretical studies at finite coverage [above around 10^{-3} ML range for $n=1$ IS in the case of Cs adsorbates on Cu(100)] have to take into account the collective effect of all the adsorbates present on the surface when considering electron scattering by a given adsorbate.

ACKNOWLEDGMENTS

A.K.K. acknowledges support from the Russian Foundation of Basic Research via Grant No. 05-02-16216. A.K.K. also gratefully acknowledges a CNRS "chercheur associé" position at the LCAM that made this collaborative work possible. V.M.S. and E.V.Ch. acknowledge the partial support from the University of the Basque Country UPV/EHU (Grant No. 9/UPV 00206.215-13639/2001), the Departamento de Educación, Universidades e Investigatión del Gobierno Vasco, the Spanish Ministerio de Ciencia y Tecnología MCyT (Grant No. FIS2004-06490-C03-01).

[1] Th. Fauster and W. Steinmann, in *Photonic Probes of Surfaces, Electromagnetic Waves: Recent Developments in Research* Vol. 2, edited by P. Halevi (North-Holland, Amsterdam, 1995), Chap. 8, p. 347.

[2] H. Petek and S. Ogawa, Prog. Surf. Sci. **56**, 239 (1997).

[3] P. M. Echenique, R. Berndt, E. V. Chulkov, Th. Fauster, A. Goldmann, and U. Höfer, Surf. Sci. Rep. **52**, 219 (2004).

[4] *Photochemistry and Photophysics on Surfaces*, edited by J. T. Yates, Jr. and H. Petek, Chem. Rev. (Washington, D.C.) V **106**, p. 1 (2006).

[5] M. C. Desjonquères and D. Spanjaard, *Concepts in Surface Science*, Springer-Verlag Series in Surface Science Vol. 40, (Springer-Verlag, Berlin, 1993).

[6] P. M. Echenique and J. B. Pendry, J. Phys. C **11**, 2065 (1978).

[7] N. V. Smith, Phys. Rev. B **32**, 3549 (1985).

[8] D. Straub and F. J. Himpsel, Phys. Rev. B **33**, 2256 (1986).

[9] M. Weinelt, J. Phys.: Condens. Matter **14**, R1099 (2002).

[10] S. L. Hulbert, P. D. Johnson, M. Weinert, and R. F. Garrett, Phys. Rev. B **33**, 760 (1986).

[11] S. L. Hulbert, P. D. Johnson, N. G. Stoffel, W. A. Royer, and N. V. Smith, Phys. Rev. B **31**, 6815 (1985).

[12] M. Roth, M. Pickel, J. Wang, M. Weinelt, and Th. Fauster, Appl. Phys. B: Lasers Opt. **74**, 661 (2002).

[13] E. V. Chulkov, I. Sarria, V. M. Silkin, J. M. Pitarke, and P. M. Echenique, Phys. Rev. Lett. **80**, 4947 (1998).

[14] P. M. Echenique, J. M. Pitarke, E. V. Chulkov, and A. Rubio, Chem. Phys. **251**, 1 (2000).

[15] S. D. Kevan, Phys. Rev. Lett. **50**, 526 (1983); Phys. Rev. B **33**, 4364 (1986); Surf. Sci. **178**, 229 (1986).

[16] S. Schuppler, N. Fischer, Th. Fauster, and W. Steinmann, Phys. Rev. B **46**, 13539 (1992).

[17] R. W. Schoenlein, J. G. Fujimoto, G. L. Eesley, and T. W. Capehart, Phys. Rev. Lett. **61**, 2596 (1988).

[18] R. W. Schoenlein, J. G. Fujimoto, G. L. Eesley, and T. W. Cape-

hart, Phys. Rev. B **43**, 4688 (1991).
[19] X. Y. Wang, R. Paiella, and R. M. Osgood, Jr., Phys. Rev. B **51**, 17035 (1995).
[20] U. Höfer, I. L. Shumay, Ch. Reuß, U. Thomann, W. Wallauer, and Th. Fauster, Science **277**, 1480 (1997).
[21] T. Hertel, E. Knoesel, M. Wolf, and G. Ertl, Phys. Rev. Lett. **76**, 535 (1996).
[22] Th. Fauster, C. Reuß, I. L. Shumay, and M. Weinelt, Chem. Phys. **251**, 111 (2000).
[23] J. Güdde and U. Höfer, Prog. Surf. Sci. **80**, 49 (2005).
[24] Ch. Reuß, I. L. Shumay, U. Thomann, M. Kutschera, M. Weinelt, Th. Fauster, and U. Höfer, Phys. Rev. Lett. **82**, 153 (1999).
[25] K. Boger, M. Weinelt, and Th. Fauster, Phys. Rev. Lett. **92**, 126803 (2004).
[26] K. Boger, Th. Fauster, and M. Weinelt, New J. Phys. **7**, 110 (2005).
[27] A. G. Borisov, J. P. Gauyacq, and A. K. Kazansky, Surf. Sci. **505**, 260 (2002).
[28] A. G. Borisov, A. K. Kazansky, and J. P. Gauyacq, Surf. Sci. **526**, 72 (2003).
[29] A. G. Borisov, J. P. Gauyacq, and A. K. Kazansky, Surf. Sci. **540**, 407 (2003).
[30] F. E. Olsson, A. G. Borisov, M. Persson, N. Lorente, A. K. Kazansky, and J. P. Gauyacq, Phys. Rev. B **70**, 205417 (2004).
[31] F. E. Olsson, A. G. Borisov, and J. P. Gauyacq, Surf. Sci. **600**, 2184 (2006).
[32] C. Cohen-Tannoudji, J. Dupont-Roc, and G. Grynberg, *Processus d'Interaction Entre Photons et Atomes* (EDP Sciences/CNRS Editions, Les Ulis, 2001).
[33] A. K. Kazansky, A. G. Borisov, and J. P. Gauyacq, Surf. Sci. **544**, 309 (2003).
[34] N. Fischer, S. Schuppler, R. Fischer, Th. Fauster, and W. Steinmann, Phys. Rev. B **47**, 4705 (1993).
[35] E. V. Chulkov, V. M. Silkin, and P. M. Echenique, Surf. Sci. **437**, 330 (1999).
[36] M. Scheffler, Ch. Droste, A. Fleszar, F. Maca, G. Wachutka, and G. Barzel, Physica B **172**, 143 (1991).
[37] J. P. Gauyacq, A. G. Borisov, and M. Bauer, Prog. Surf. Sci. **82**, 244 (2007).
[38] S. Å. Lindgren, L. Walldén, J. Rundgren, P. Westrin, and J. Neve, Phys. Rev. B **28**, 6707 (1983).
[39] S. Å. Lindgren and L. Walldén, Solid State Commun. **25**, 13 (1978).
[40] J. N. Bardsley, Case Stud. At. Phys. **4**, 299 (1974).
[41] L. Kleinman and D. M. Bylander, Phys. Rev. Lett. **48**, 1425 (1982).
[42] M. C. Xu, T. Iimori, and F. Komori, Surf. Sci. **539**, L549 (2003).
[43] L. Hedin and S. Lundqvist, Solid State Phys. **23**, 1 (1969).
[44] V. M. Silkin, J. M. Pitarke, E. V. Chulkov, and P. M. Echenique, Phys. Rev. B **72**, 115435 (2005).
[45] E. V. Chulkov, A. G. Borisov, J. P. Gauyacq, D. Sanchez-Portal, V. M. Silkin, V. P. Zhukov, and P. M. Echenique, Chem. Rev. (Washington, D.C.) **106**, 4160 (2006).
[46] J. Sjakste, A. G. Borisov, J. P. Gauyacq, and A. K. Kazansky, J. Phys. B **37**, 1593 (2004).
[47] W. Demtröder, *Laser Spectroscopy, Basic Concepts and Instrumentation* (Springer-Verlag, Berlin, 1982).
[48] B. Simon, Ann. Phys. (Paris) **97**, 279 (1976).
[49] A. G. Borisov, A. K. Kazansky, and J. P. Gauyacq, Phys. Rev. B **65**, 205414 (2002).
[50] J. P. Gauyacq, A. G. Borisov, and A. K. Kazansky, Appl. Phys. A: Mater. Sci. Process. **78**, 141 (2004).
[51] V. S. Stepanyuk, A. N. Klavsyuk, L. Niebergall, and P. Bruno, Phys. Rev. B **72**, 153407 (2005).
[52] B. Lazarovits, L. Szunyogh, and P. Weinberger, Phys. Rev. B **73**, 045430 (2006).
[53] F. E. Olsson, M. Persson, A. G. Borisov, J. P. Gauyacq, J. Lagoute, and S. Fölsch, Phys. Rev. Lett. **93**, 206803 (2004).
[54] L. Limot, E. Pehlke, J. Kröger, and R. Berndt, Phys. Rev. Lett. **94**, 036805 (2005).
[55] C. Liu, I. Matsuda, R. Hobara, and S. Hasegawa, Phys. Rev. Lett. **96**, 036803 (2006).
[56] J. Kröger, L. Limot, H. Jensen, R. Berndt, S. Crampin, and E. Pehlke, Prog. Surf. Sci. **80**, 26 (2005).